

THE UDF05 FOLLOW-UP OF THE HUBBLE ULTRA DEEP FIELD. III. THE LUMINOSITY FUNCTION AT $z \sim 6$ ¹

JIAN SU^{2,3}, MASSIMO STIAVELLI³, PASCAL OESCH^{4,5,6}, MICHELE TRENTI⁷, EDDIE BERGERON³, LARRY BRADLEY³, MARCELLA CAROLLO⁴, TOMAS DAHLEN³, HENRY C. FERGUSON³, MAURO GIAVALISCO⁸, ANTON KOEKEMOER³, SIMON LILLY⁴, RAY A. LUCAS³, BAHRAM MOBASHER⁹, NINO PANAGIA^{3,10,11}, CHERYL PAVLOVSKY³

Draft version November 13, 2021

ABSTRACT

In this paper, we present a derivation of the rest-frame 1400Å luminosity function (LF) at redshift six from a new application of the maximum likelihood method by exploring the five deepest *HST/ACS* fields, i.e., the HUDF, two UDF05 fields, and two GOODS fields. We work on the latest improved data products, which makes our results more robust than those of previous studies. We use un-binned data and thereby make optimal use of the information contained in the dataset. We focus on the analysis to a magnitude limit where the completeness is larger than 50% to avoid possibly large errors in the faint end slope that are difficult to quantify. We also take into account scattering in and out of the dropout sample due to photometric errors by defining for each object a probability that it belongs to the dropout sample. We find the best fit Schechter parameters to the $z \sim 6$ LF are: $\alpha = 1.87 \pm 0.14$, $M_* = -20.25 \pm 0.23$, and $\phi_* = 1.77^{+0.62}_{-0.49} \times 10^{-3} \text{ Mpc}^{-3}$. Such a steep slope suggests that galaxies, especially the faint ones, are possibly the main sources of ionizing photons in the universe at redshift six. We also combine results from all studies at $z \sim 6$ to reach an agreement in 95% confidence level that $-20.45 < M_* < -20.05$ and $-1.90 < \alpha < -1.55$. The luminosity density has been found not to evolve significantly between $z \sim 6$ and $z \sim 5$, but considerable evolution is detected from $z \sim 6$ to $z \sim 3$.

Subject headings: galaxies: evolution — galaxies: formation — galaxies: high-redshift — galaxies: luminosity function — methods: data analysis

1. INTRODUCTION

Deep imaging surveys, such as the Great Observatories Origins Deep Survey (GOODS, Giavalisco et al. 2004) and the Hubble Ultra Deep Field (HUDF, Beckwith et al. 2006), have been extensively analyzed to study galaxy properties out to the reionization epoch. The rest-frame ultraviolet (UV) galaxy luminosity function (LF) is measured for samples of Lyman break galaxies (LBGs) and used to detect cosmic evolution. The consensus that has developed is that a considerable increase in the space-density of galaxies at the bright end

of the LF occurs from redshift $z \sim 6$ (Bunker et al. 2004; Yan & Windhorst 2004; Beckwith et al. 2006; Bouwens et al. 2006)¹² to $z \sim 3$ (e.g., Steidel et al. 1999). However, there are still some discrepancies in the interpretation of this evolution, in terms of density, slope, luminosity, or a combination of these. Bunker et al. (2004) undertake a photometric analysis of the HUDF i_{775} -dropouts and propose that the density increases six-fold from $z \sim 6$ to $z \sim 3$, in agreement with Beckwith et al. (2006). Yan & Windhorst (2004) push the detection limit deeper to magnitude 30, finding a steeper faint slope at $z \sim 6$ compared to $z \sim 3$ by 0.2-0.3. Furthermore, Bouwens et al. (2006) estimate corrections to the measured quantities to account for various observational effects and conclude that the intrinsic luminosity is ~ 0.8 mag fainter at $z \sim 6$. Their conclusions remain qualitatively unchanged after Reddy & Steidel (2009) recently revisit the LF parameters at $z \sim 3$. On the other hand, ground-based observations, e.g., McLure et al. (2009), find an even stronger luminosity evolution.

Different measurements of the luminosity density (LD) or star formation rate (SFR) also give somewhat different results (e.g., Bunker et al. 2004; Bouwens et al. 2006). It is important to establish whether these observed differences are due to intrinsic differences in the evolution of different galaxy populations or due to issues with the derivation of the LF.

Spectroscopic confirmations of $z \sim 6$ galaxies, e.g., Malhotra et al. (2005), Dow-Hygelund et al. (2007), Hathi et al. (2008) and Vanzella et al. (2009), have already proven the effectiveness and robustness of the

¹ Based on observations made with the NASA/ESA Hubble Space Telescope, obtained at the Space Telescope Science Institute, which is operated by the Association of Universities for Research in Astronomy, Inc., under NASA contract NAS 5-26555. These observations are associated with program #10632 and #11563.

² Department of Physics and Astronomy, Johns Hopkins University, Baltimore, MD 21218, USA; sujian@pha.jhu.edu

³ Space Telescope Science Institute, Baltimore, MD 21218, USA

⁴ Institute of Astrophysics, ETH Zurich, CH - 8093 Zurich, Switzerland

⁵ UCO/Lick Observatory, University of California, Santa Cruz, CA 95064

⁶ Hubble Fellow

⁷ University of Colorado, CASA, Dept. of Astrophysical & Planetary Sciences, 389-UCB, Boulder, CO 80309, USA

⁸ Department of Astronomy, University of Massachusetts, Amherst, MA 01003, USA

⁹ Department of Physics and Astronomy, University of California, Riverside, CA 92521, USA

¹⁰ INAF- Osservatorio Astrofisico di Catania, Via S. Sofia 78, I-95123 Catania, Italy

¹¹ Supernova Ltd., OYV 131, Northsound Road, Virgin Gorda, British Virgin Islands

¹² The results of these groups are summarized in Table 4.

dropout technique in selecting LBGs. However, the faint LBGs, which are essential to determining the faint-end slope of the LF, have not been spectroscopically confirmed because they require impractically long exposure time on large telescopes.

Therefore, to improve upon the previous studies of the $z \sim 6$ LF and to establish its form, a number of difficult issues should be considered. (a) Optimal use of the data: a single field provides us with only a handful of candidates so that some magnitude intervals contain only very few objects. Thus, it is very important to keep all the information. In order to do so, we use un-binned data. (b) Completeness of the catalogs: the correction to the number of objects observed at faint magnitudes is significant due to the detection incompleteness. We adopt a more moderate magnitude limit than other groups in order to avoid possible uncertainties brought by large corrections. (c) Photometric errors and biases: a strict color cut used for i_{775} -dropout selection may lose real LBGs and is affected by contaminants. For each galaxy within or outside the selection window, we explicitly consider its probability of being an actual LBG by assuming a Gaussian distribution for the photometric error.

On the basis of the HUDF images (Beckwith et al. 2006, hereafter paper I), the UDF05 images (Oesch et al. 2007, hereafter paper II), and the HUDF09 images (Oesch et al. 2010; Bouwens et al. 2010a), we are now in the position to study properties of LBGs from $z \sim 0$ to beyond $z \sim 8$ utilizing *Hubble Space Telescope's* (*HST*) unparalleled deep optical and infrared (IR) view. In this paper, we plan to further develop techniques to derive the LF at $z \sim 6$ using the procedures used for $z \sim 5$ galaxies in paper II. In particular, we apply the maximum likelihood (ML) method, which is independent of clustering in our sample, to derive the LF and examine whether star forming galaxies, especially the faint ones, are responsible for re-ionizing or keeping the universe ionized at $z \sim 6$.

We adopt Λ CDM cosmology: $\Omega_M = 0.3$, $\Omega_\Lambda = 0.7$, and $H_0 = 70 \text{ km s}^{-1} \text{ Mpc}^{-1}$. Magnitudes are in the AB system.

2. DATA

We work on five *HST*/ACS deep fields in four broad bands: F435W (B_{435}), F606W (V_{606}), F775W (i_{775}), and F850LP (z_{850}). We use the most recent and updated version of the data, namely: GOODS South (GOODS-S) & GOODS North (GOODS-N) v2.0 data by Giavalisco et al. (2008), the HUDF data from paper I, HUDF NICP12 from paper II, and HUDF NICP34 processed in this work. PyRAF tasks Multidrizzle and Tweakshifts (Koekemoer et al. 2006) help precisely align the images, and SExtractor (Bertin & Arnouts 1996) is run in double-image mode with z_{850} as the detection band to generate the catalogs. Our survey covers $\sim 350 \text{ arcmin}^2$ to a magnitude limit of $z_{850} \sim 29$, identifying ~ 1100 LBG candidates at $z \sim 6$, with an average number of 350 per realization, as shown in Table 1.

We have not made use of the WFC3/IR data that are becoming available on these fields for two main reasons: (a) The IR data are not available over the full fields, especially only a small portion of the GOODS has been covered. This would force us to reduce the sample size greatly. (b) We think an important component of this

work is a comparison with other published results which are based on the simple one color selection rather than a full two-color selection. We do make a quick check of the IR information in the HUDF in Section 3.1 and will leave a full investigation for future work.

We also do not use ground based data for two main reasons: (a) The two GOODS fields are already large enough to provide good constraints on galaxies brighter than the knee of the Schechter function. (b) We prefer to work with a homogenous data set in terms of filters and detector QE curves.

3. LUMINOSITY FUNCTION OF LBGs AT $z \sim 6$

The completeness function $C(m)$ (m is the apparent/detected magnitude) and the selection function $S(m, z)$ (z is the redshift) are measured by performing recovery simulations in the same way as in paper II, i.e., by inserting artificial galaxies into our science images and rerunning SExtractor with the same setup as for the original catalog generation. We use a β -distribution -2.2 ± 0.4 (Stanway et al. 2005) and a size distribution following a scaling of $(1+z)^{-1}$ as in Ferguson et al. (2004). For each redshift bin $\delta z = 0.1$, we thus compute the color a galaxy would have with the randomly chosen β -value and insert it in the images. The input magnitudes are following a flat distribution from 24–29, but the selection function is given at observed magnitudes, simply by computing the fraction of galaxies that we insert with the measured output magnitude which is selected by the i_{775} -dropout criteria. $C(m)dm$ is defined as the probability that a galaxy of m in the images is selected in the catalog, which depends strongly on SExtractor parameters such as DEBLEND. Thus, it is important that the recovery simulations are done using the same SExtractor parameters used to derive the catalog. $S(m, z)dmdz$ represents the probability that a LBG at a given redshift z and at a given observed magnitude m satisfies the selection criteria. Naturally, the product of these two functions $C(m)S(m, z)dmdz$ is the probability that a galaxy at redshift z is detected with magnitude m AND selected as a LBG.

The UV LF can be expressed in Schechter form as,

$$\phi(M) = (0.4 \ln 10) \phi_* 10^{0.4(1+\alpha)(M_* - M)} \exp[-10^{0.4(M_* - M)}] \quad (1)$$

with the absolute magnitude $M = m - DM(z) - K_{cor}(z)$, where $DM(z)$ is the distance modulus and $K_{cor}(z)$ is the K-correction from observed z_{850} to rest-frame 1400 Å.

Binned data were initially utilized by many groups to derive the shape of the LF. The observed number of LBGs within the apparent magnitude bin $m_l < m < m_u$ is predicted as

$$N_i = \int dz \frac{dV_C}{dz}(z) \int_{m_l}^{m_u} dm C(m) S(m, z) \phi(M(m, z); \phi_*, M_*, \alpha) \quad (2)$$

where dV_C/dz is the comoving volume element of the survey. Binning may lose information, and lead to biased results dependent on the bin size. At the same time, having very few luminous candidates in current high- z surveys, there is uncertainty about the numbers in the bright bins since the candidates could jump into adjacent bins due to photometric errors. Simulations by Trenti & Stiavelli (2008) show that binning is likely to affect the confidence

regions for the best-fitting parameters.

To overcome these drawbacks, in this section we present an improved approach based on the ML method (Fisher 1922; Sandage, Tammann, & Yahil 1979, STY) to make optimal use of every possible LBG in the fields. As also pointed out by Trenti & Stiavelli (2008), the STY ML estimator relies essentially on un-binned data. We determine the shape of the LF by exploring every single detected dropout. First, we find the probability for each galaxy that it could be selected as a LBG, considering the photometric uncertainty of the catalogs (Section 3.2). Second, we choose galaxies randomly by the above probability and run our ML process (Section 3.3). Third, we repeat the above step enough times to achieve convergence.

3.1. Selection Criteria

We adopt the i_{775} -dropout selection criteria from paper I, i.e.,

$$i_{775} - z_{850} > 1.3, \quad (3)$$

$$S/N(z_{850}) > 5, \quad (4)$$

$$S/N(V_{606}) < 2 \text{ or } V_{606} - z_{850} > 2.8. \quad (5)$$

The dominant criterion, i.e., the SExtractor MAG_ISO color $i_{775} - z_{850} > 1.3$, will be further discussed in Section 3.2. The signal-to-noise ratio $S/N(z_{850}) > 5$ is demanded for each candidate to largely avoid interlopers (later this subsection) or slope steepening (Appendix), and to be consistent in comparing with $z \sim 3$ results from Steidel et al. (1999) and with $z \sim 5$ results in paper II. The photometric errors also take into account the correlated errors present in the images as discussed in paper II. In addition, we require for CLASS_STAR < 0.75 if the MAG_AUTO magnitude $z_{850} < 28.0$ for the HUDF, < 27.5 for the UDF05, and < 26.5 for the GOODS in order to remove stellar contamination at the bright end (e.g., Bouwens et al. 2006, and paper II). Only galaxies with $C(m) > 0.5$ have been included to avoid large uncertainty corrections (Table 2). The selection has been proven to be very efficient and effective. All the spectroscopically confirmed $i_{775} - z_{850} > 1.3$ $z \sim 6$ LBGs through the HUDF/GOODS follow-up surveys (e.g., Malhotra et al. 2005; Vanzella et al. 2009) satisfy our criteria, with only one exception, and no Galactic star could pass the CLASS_STAR test.

We have estimated the possible fraction of interlopers by applying our selection criteria of equations (3)-(5) to a library of ~ 3000 synthetic SEDs built on Bruzual-Charlot models (Bruzual & Charlot 2003), adopting the LF derived by Steidel et al. (1999) at $z \sim 3$ and no evolution. The models include the effects of intergalactic absorption (Madau 1995), and span a wide range of metallicities (0.04 - $2.5 Z_{\odot}$), dust reddening (no extinction, or eight values logarithmically spaced between $A_V = 0.05$ and 6.4), emission lines (no lines or lines computed from first principles from UV SED for Hydrogen and fit to Cloudy models for metal lines), and different star formation histories (burst, constant at fixed metallicity, constant at evolving metallicity without infall or with infall, two component models with an old component and a young one which may include emission lines). We consider 18 ages logarithmically spaced between 1 Myrs and 18 Gyrs. And no model older than

the universe is included. We can see from the resulting redshift distribution (Fig. 1) that there is a lower redshift population $z \sim 1, 2$ of galaxies that may be selected as LBGs at $z \sim 6$ due to the aliasing between the Lyman break and the 4000\AA break (See e.g., Dahlen et al. 2010, for more discussions). In Fig. 2, we have identified our $i_{775} - z_{850} > 1.3$ candidates detected by the WFC3 F105W (Y_{105}) band in the HUDF to verify that our sample does not have many interlopers.

3.2. f -factor

Photometric scatter introduces large uncertainties in numbers and magnitudes of the LBG candidates, and therefore, in determined properties of the LF. If a strict color cut such as $i_{775} - z_{850} > 1.3$ was applied, the impact of photometric errors would not be fully explored, and many real LBGs with a little bluer measured color may be missed due to photometric errors. A relaxed cut, e.g., $i_{775} - z_{850} > 0.9$, on the other hand, suffers from larger contaminations. For example, Malhotra et al. (2005) found five objects at intermediate redshifts and four intrinsic $z \sim 6$ galaxies within $0.9 < i_{775} - z_{850} < 1.3$, which means the contamination rate in the relaxed color window may be as high as $5/(5+4) = 56\%$.

To account for this effect, we calculate the probability that each object is an LBG, which decides how often it could contribute to the later ML process. If $p(m)dm$ is the probability that a galaxy is of magnitude m in the catalog, then the f -factor of $i_{775} - z_{850} > 1.3$ LBG candidates is defined as:

$$f = \int dz_{850} di_{775} p(z_{850})p(i_{775}) \quad (6)$$

where the integration of i_{775} is taken over $i_{775} - z_{850} > 1.3$. The real magnitude m is assumed to be a Gaussian distribution around its cataloged magnitude m_c (See Appendix for details). In practice, one could find the values of f -factor with a Monte Carlo method by simply generating Gaussian distributed magnitudes repeatedly to see how often the $i_{775} - z_{850} > 1.3$ color would be satisfied. A $2\text{-}\sigma$ magnitude limit is adopted if there is no detection in the i_{775} -band.

It is easy to see that $f > 0.5$ when the cataloged $i_{775} - z_{850} > 1.3$ while $f < 0.5$ when the cataloged $i_{775} - z_{850} < 1.3$, and $f = 0.01$ corresponds to the cataloged $i_{775} - z_{850} \sim 0.9$ when the z_{850} and i_{775} errors are both 0.2. All $f \geq 0.01$ galaxies are used in the subsequent ML analysis, i.e., 1% chance of being included in one realization. Table 1 shows that essentially about 25% - 50% candidates in each field will participate in one realization, which brings our sample in agreement with other groups within the magnitude window in study, such as Bouwens et al. (2007). (See Fig. 3 and Table 3.)

3.3. V -Matrix

Due to the unique long tail of the ACS z_{850} -filter, the K-correction can be as large as 2.2 mag at $z = 5.7$ and goes down to 0.3 mag at $z = 7.0$. Thus, with distance modulus varying by 0.5 mag there could be a 2.4-mag scatter in UV rest frame absolute magnitudes in realizations at $5.7 < z < 7$ for any given observed z_{850} -magnitude. In other words, the relation between M and m is very uncertain. Therefore, applicable at where M

is relatively insensitive to redshift or the redshift span is relatively small, the effective volume V_{eff} technique does not fit in our case. This forces us to seek a new formalism.

We define the apparent LF as

$$\Phi(m) = \frac{C(m)}{V_{eff}} \int dz S(m, z) \frac{dV_C}{dz}(z) \phi(M; m, z) \quad (7)$$

and it does not need to be of Schechter form. The V-matrix is therefore,

$$V(m, z) \equiv C(m) S(m, z) \frac{dV_C}{dz}(z) \quad (8)$$

and $V_{eff}(m) = \int dz V(m, z)$. We maximize the likelihood function $\ln L = \sum_i \ln p(m_i)$ where

$$\begin{aligned} p(m_i) &= \Phi(m_i) / \int dm \Phi(m) \\ &= \int dz V(m_i, z) \phi(M_i) / \int \int dmdz V(m, z) \phi(M) \end{aligned} \quad (9)$$

The integrations are always taken over the region of interest, for example for the HUDF, $5.7 < z < 7.0$ and $24.0 < m < 28.5$. (The bright limit is introduced for calculations only when there is no candidate detected beyond this magnitude, and an even brighter limit will not affect the results since the LF is greatly suppressed at this end.) $C(m)$ has been included in the calculation of $V(m, z)$ so that there is no additional completeness correction factor in $p(m_i)$.¹³

When combining different fields, e.g., the GOODS and the HUDF, no additional rescaling factor is needed in the ML method (Trenti & Stiavelli 2008). The inputs to the ML process are the V-matrix and the magnitudes m of selected candidates. In each realization, candidates are selected from the pool in a probability as to their f -factor. The outputs are M_* and α in as many as possible realizations, when the averages and errors have been convergent. The uncertainty of m considered in the ML process only yields minor errors when several hundreds of galaxies are surveyed (Appendix). ϕ_* is determined by χ^2 fit to the observed LBG densities with respect to the 1- σ 2-parameter contour of M_* and α .

The LF parameters we derive for $z \sim 6$ are: $\alpha = -1.87 \pm 0.14$, $M_* = -20.25 \pm 0.23$, and $\phi_* = 1.77_{-0.49}^{+0.62} \times 10^{-3} \text{ Mpc}^{-3}$, as illustrated in Fig. 4. We notice our faint end slope α is slightly steeper than that from some other studies. This could partly be caused by a steeper slope at $z \sim 7$ (e.g., Oesch et al. 2010; Trenti et al. 2010) since we include up to $z = 7$ LBGs in our estimate of the $z \sim 6$ LF.

3.4. Evolution of ϕ_*

Since we are investigating a relatively large redshift range $5.7 < z < 7.0$ and finding indication of LF evolution, it is a good sanity check for us to explicitly consider the effect of evolving LF parameters. Assuming M_* and α are uniform in this redshift range, we assign a linear evolution $\phi_*(z) = \phi_*(6.3)[1 - \frac{z}{7}(z - 6.3)]$ and

¹³ We note that Marshall (1985) adopted a similar approach to ours and he did not have to take the integration of redshift as shown above since the redshifts of their objects were already known.

repeat the analysis described in Section 3.1 - 3.3. We find that $\alpha = -1.92 \pm 0.13$, $M_* = -20.22 \pm 0.21$. The closeness to our derived parameters for no evolution, i.e., $\alpha = -1.87 \pm 0.14$ and $M_* = -20.25 \pm 0.23$, shows that our results are robust with respect to an evolution of the LF normalization within the redshift range of i_{775} -dropouts

3.5. Evolution of M_*

Similar considerations to those in the previous subsection lead us to explore a variation of M_* within the i_{775} -dropout redshift window. We do so by assigning $M_*(z) = M_*(5.9) + 0.36(z - 5.9)$ (Bouwens et al. 2007; Oesch et al. 2010) while keeping uniform values of α and ϕ_* . We find $\alpha = -1.91 \pm 0.08$, which is also within one sigma of our non-evolving derivation.

4. COMPARISON TO OTHER RESULTS

We have verified the internal consistency and robustness of our results and we are now ready to compare them to other studies.

4.1. Most Probable $z \sim 6$ LF

To deal with the weighted average of results from different groups, we follow Press (1996). The probability of getting observed variable(s) H_0 from data or measurements D is

$$P(H_0|D) \propto \prod_i (P_{Gi} + P_{Bi}) \quad (10)$$

Here $P_{Gi} \sim \frac{1}{\sigma_i} \exp[-\frac{(H_i - H_0)^2}{2\sigma_i^2}]$ and $P_{Bi} \sim \frac{1}{S} \exp[-\frac{(H_i - H_0)^2}{2S^2}]$ are the probability distributions of ‘‘good’’ and ‘‘bad’’ measurements, respectively, where i denotes different measurements, and S should be assigned to be large enough to ensure that measurements do not conflict with each other. When extending this method to two-dimensional analysis, we also consider the correlation between M_* and α (Fig. 4). Press (1996) puts almost no weight on those measurements without errors where $P_{Gi} = 0$ and P_{Bi} is widely spread. Instead, we assume a moderate error of 0.3 for those six groups, i.e., Bouwens et al. (2004), Bunker et al. (2004), Dickinson et al. (2004), Yan & Windhorst (2004), Malhotra et al. (2005), and paper I. Combined with the other four measurements providing errors, i.e., Bouwens et al. (2006), Bouwens et al. (2007), McLure et al. (2009), and this work, we find there is about a 95% chance that $-20.45 < M_* < -20.05$ and $-1.90 < \alpha < -1.55$, assuming all the current studies are independent and correct. (See Table 4 and Fig. 5.)

4.2. $z \sim 5$ LBGs LF revisited

In order to further test the method used here, we derive the faint end slope of the $z \sim 5$ LBG LF using the same catalogs and the same selection criteria as those in paper II. To study the HUDF and NICP12 data that lack enough bright candidates to determine M_* , we fix $M_* = -20.7$ to find $\alpha = -1.72 \pm 0.04$, which is in agreement with the previous results (their Table 3). Thus, our method, designed to deal with the varying K-correction in z_{850} and to account for additional uncertainties, is equivalent to our previous method in the simpler V_{606} -dropout case.

4.3. $z = 3 \sim 6$ Luminosity Density

The luminosity density (LD) at redshift z equals $\int L\phi(L)dL = L_*(z)\phi_*(z)\int_{x_0}^{\infty} x^{1+\alpha}e^{-x}dx$, where $x = L/L_*(z)$. We find there is considerable evolution between $z \sim 6$ and $z \sim 3$, but no statistically significant evolution between $z \sim 6$ and $z \sim 5$. More details are in Table 5 and Fig. 7 where $x_0 = aL_*(3)/L_*(z)$ and $a=0.3,0.2,0.04$. At lower redshifts there are fewer recombinations in the diffuse medium and therefore the required flux density to keep the universe ionized increases with increasing redshift. If the universe has finished reionizing at $z \sim 6$, then it will be kept ionized at $z \sim 5$ since the required LD at $z \sim 5$ is less than that at $z \sim 6$ and the observed ones are close to each other.

5. CONCLUSIONS

In this paper, we have reported the results of a study of a large sample of faint LBGs in the redshift interval $5.7 < z < 7.0$. Working on the five deepest *HST* fields with their most updated data, we account for the effect of photometric errors by introducing the factor f as the probability of each galaxy to be an LBG. We employ un-binned data to keep all the information and to avoid bias, and we develop a modified ML process to reduce the effect of the uncertain relation between M and m . Our best-fitting Schechter function parameters of the rest-frame 1400Å LF at redshift $z \sim 6$ are: $\alpha = -1.87 \pm 0.14$, $M_* = -20.25 \pm 0.23$, and $\phi_* = 1.77_{-0.49}^{+0.62} \times 10^{-3} \text{ Mpc}^{-3}$, which suggest evolution of M_* , possible steepening of α , and no change of ϕ_* compared to their values at $z \sim 3$. Such a steep slope suggests that galaxies, especially the faint ones, are possibly the main sources of ionizing photons in the universe at redshift six (Stiavelli et al. 2004). Combining ten previous studies at $z \sim 6$ with the

extended Press method, we find that the most probable LF favors $-20.45 < M_* < -20.05$ and $-1.90 < \alpha < -1.55$ at the 95% confidence level. The LD has been found not to evolve significantly between $z \sim 6$ and $z \sim 5$, but considerable change is detected from $z \sim 6$ to $z \sim 3$.

If α remains constant from $z \sim 6$ to $z \sim 3$ as stated by e.g., Bouwens et al. (2007) and Reddy & Steidel (2009), it will be difficult to tell the intrinsically evolving parameter, M_* or ϕ_* , from faint LBGs only, while too few bright LBGs are found due to the limited area of current deep surveys. Ground-based surveys such as the Subaru Deep Field (Shimasaku et al. 2005; McLure et al. 2009) are extremely efficient in detecting bright LBGs in a large field of view and might clarify whether M_* or ϕ_* alone is not responsible for the change of LF, while splitting the z_{850} -band into two separate bands may be useful to isolate the effect of a possible slope steepening (Shimasaku et al. 2005). We look forward to including IR data from WFC3 on board *HST* to improve the selection of $z \sim 6$ LBG candidates, and the bright end of the LF will be better determined when the data from CANDELS/ERS (e.g., Bouwens et al. 2010b) and the BoRG survey (Trenti et al. 2011) are becoming available.

JS and MS have been partially supported by NASA grant NAG 5-12458. PO is supported by NASA through Hubble Fellowship grant HF-51278.01. Support for program #10632 and #11563 was provided by NASA through a grant from the Space Telescope Science Institute, which is operated by the Association of Universities for Research in Astronomy, Inc., under NASA contract NAS 5-26555.

APPENDIX

MORE ABOUT PHOTOMETRIC SCATTER AND FLUX BOOSTING

We assume the photometric scatter is in a Gaussian distribution, thus the probability of a galaxy arriving on the detector as magnitude m but cataloged in m' equals

$$G(m, m', \sigma) = \frac{1}{\sqrt{2\pi\sigma^2}} \exp\left[-\frac{(m - m')^2}{2\sigma^2}\right] \quad (\text{A1})$$

and the measured LF will be

$$\phi'(m) = \int \phi(m')G(m, m', \sigma)dm' \quad (\text{A2})$$

where ϕ is the actual LF, i.e., Equation (7) in Section 3.3.

When the photometric error σ is very small, G takes the limit of the Dirac function and it is always true $\phi' \equiv \phi$. When the surveys are pushed close to the detection limit, σ is not negligible and also far from uniform in the magnitude window. To satisfy $S/N = 10$ at $m = m_*$ and $S/N = 5$ at $m = m_* + 2.5$, a guess would be

$$\sigma(m) = \frac{2.5}{\ln 10} \frac{1}{2(m_* - m) + 10} \quad (\text{A3})$$

Simulations show that the effect of flux boosting from fainter magnitudes outside our selection window is negligible. But as shown in Table 6, if $\sigma(m)$ increases much faster with m , or if lower S/N candidates are included, there will be considerable steepening at the faint end due to the photometric scattering. We simulate 4000 objects according to the given LF parameters, i.e., m_* is fixed and $\alpha = -1.7$ in $[m_* - 3.5, m_* + 4.5]$. Their magnitude errors are assumed to be in the form of $10^{0.3(m - m_*)}$ which comes from the real data of the HUDF. For each realization, the change of magnitudes brought by their errors will also change their detected S/N. We choose those with the $S/N > 5$ and lying within $[m_* - 2.5, m_* + 2.5]$ to determine the slope. This process repeats for different combinations of $S/N > 5, 7, 9$ and

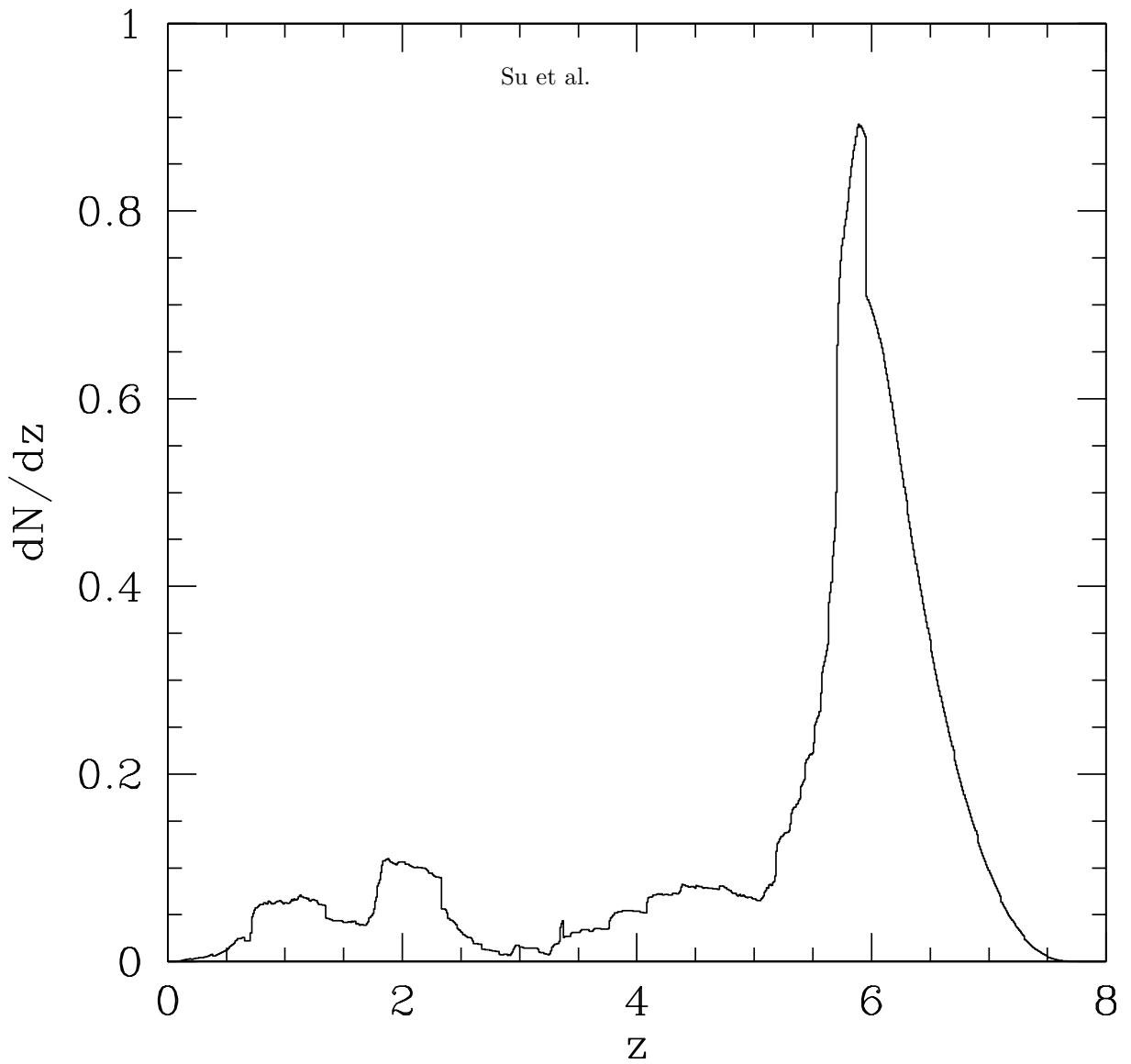


FIG. 1.— Predicted redshift distribution for i_{775} -dropouts as derived assuming synthetic SEDs and a non-evolving LF in the redshift window $5.7 < z < 7$. The total interloper fraction is estimated to be 24% and is primarily contributed by lower redshift galaxies selected as LBGs due to the aliasing between the Lyman break and the 4000Å break. The model is pessimistic and at the relatively bright end ($z_{850} < 27.5$) comparison with Malhotra et al. (2005) shows a factor of two fewer interlopers than predicted by the model.

$\alpha = -1.5, -1.7, -1.9$. We can see from Table 6 that if the S/N is kept > 5 , the steepening of the faint end slope by the flux boosting is less than 0.1.

REFERENCES

- Beckwith, S. V. W., et al. 2006, *AJ*, 132, 1729 (paper I)
 Bertin, E. & Arnouts, S. 1996, *A&A*, 117, 393
 Bouwens, R. J., et al. 2004, *ApJ*, 606, L25
 Bouwens, R. J., et al. 2006, *ApJ*, 653, 53
 Bouwens, R. J., et al. 2007, *ApJ*, 670, 928
 Bouwens, R. J., et al. 2010a, *ApJ*, 709, L133
 Bouwens, R. J., et al. 2010b, arXiv1006.4360
 Bruzual, G., & Charlot, S. 2003, *MNRAS*, 344, 1000
 Bunker, A. J., et al. 2004, *MNRAS*, 355, 374
 Dahlen, T., et al. 2010, *ApJ*, 724, 425
 Dickinson, M., et al. 2004, *ApJ*, 600, L99
 Dow-Hygelund, C. C., et al. 2007, *ApJ*, 660, 47
 Fisher, R. A. 1922, *Philos. Trans. Roy. Soc. London Ser. A*, 222, 309
 Ferguson, H. C., et al. 2004, *ApJ*, 600, L107
 Giavalisco, M., et al. 2004, *ApJ*, 600, L93
 Giavalisco, M. and the GOODS Team, 2008, in preparation
 Hathi, N. P., et al. 2008, *ApJ*, 673, 686
 Koekemoer, A. M., et al. 2006, *The 2005 HST Calibration Workshop*, 423
 Madau, P. 1995, *ApJ*, 441, 18
 Malhotra, S., et al. 2005, *ApJ*, 626, 666
 Marshall, H. L. 1985, *ApJ*, 299, 109
 McLure, R. J., et al. 2009, *MNRAS*, 395, 2196
 Oesch, P. A., et al. 2007, *ApJ*, 671, 1212 (paper II)
 Oesch, P. A., et al. 2010, *ApJ*, 709, L160
 Press, W. H. 1996, astro-ph/9604126
 Reddy, N. A., & Steidel, C. C. 2009, *ApJ*, 692, 778
 Sandage, A., et al. 1979, *ApJ*, 232, 352
 Shimasaku, K., et al. 2005, *PASJ*, 57, 447
 Stanway, E. R., et al. 2005, *MNRAS*, 359, 1184
 Steidel, C. C., et al. 1999, *ApJ*, 519, 1
 Stiavelli, M., et al. 2004, *ApJ*, 610, L1
 Trenti, M., & Stiavelli, M. 2008, *ApJ*, 676, 767
 Trenti, M., et al. 2010, *ApJ*, 714, L202
 Trenti, M., et al. 2011, *ApJ*, 727, L39
 Vanzella, E., et al. 2009, *ApJ*, 695, 1163
 Yan, H., & Windhorst, R. A. 2004, *ApJ*, 612, L93

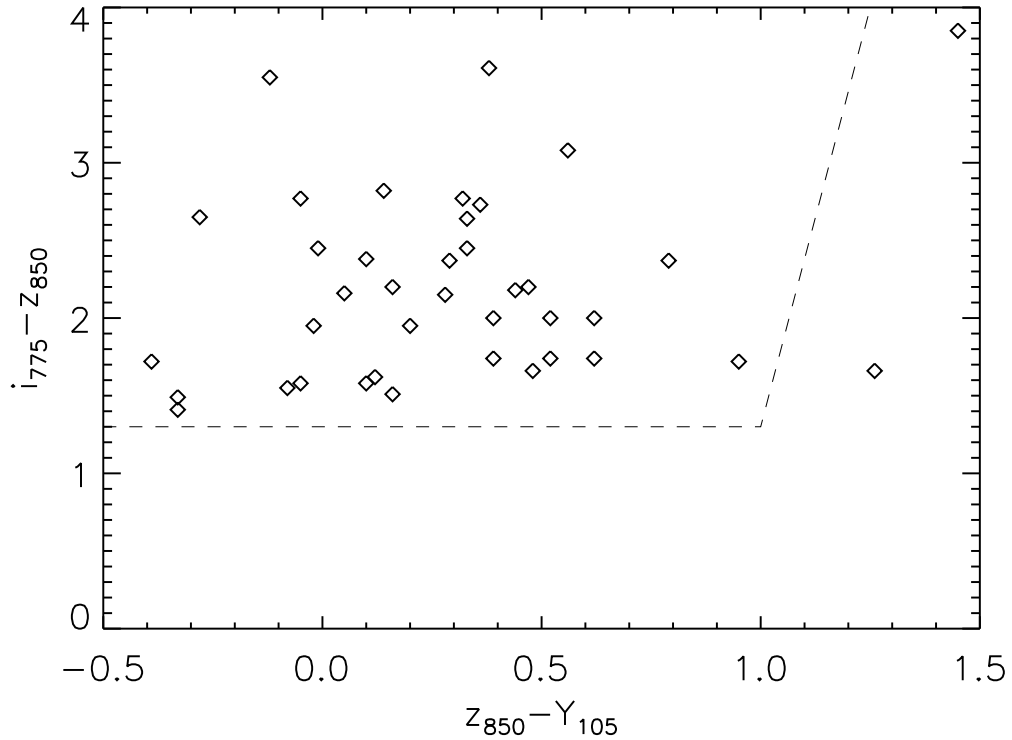


FIG. 2.— Color-color diagram of the HUDF $i_{775} - z_{850} > 1.3$ candidates. z_{850} image is rescaled to match Y_{105} to get the $z_{850} - Y_{105}$ color. The dash lines give a possible i_{775} -dropout selection criterion, namely $i_{775} - z_{850} > 1.3$ and $z_{850} - Y_{105} < 1 + 0.09(i_{775} - z_{850} - 1.3)$.

TABLE 1
DROPOUTS IN OUR SAMPLE

	HUDF	GOODS-S	GOODS-N	NICP12	NICP34
N_{tot}^a	115	373	502	120	54
N_s^b	58.1 ± 2.3	103.1 ± 6.5	116.2 ± 7.0	33.9 ± 3.0	23.5 ± 5.7

^a Total number of galaxies in our candidates pool.

^b Average number of galaxies in one realization.

TABLE 2
COMPLETENESS OF THE FIELDS

z_{850}^a	HUDF	NICP12	NICP34	GOODS
24.25	0.95	0.95	0.96	0.96
24.75	0.94	0.94	0.95	0.96
25.25	0.93	0.94	0.94	0.95
25.75	0.92	0.93	0.93	0.94
26.25	0.91	0.92	0.92	0.86
26.75	0.89	0.91	0.87	0.61
27.25	0.87	0.86	0.70	0.30
27.75	0.79	0.72	0.43	0.10
28.25 ^b	0.60	0.47	0.19	...
28.75	0.37	0.23	0.07	...

^a Central bin magnitude.

^b Only data with completeness above half are considered to avoid large uncertainty corrections.

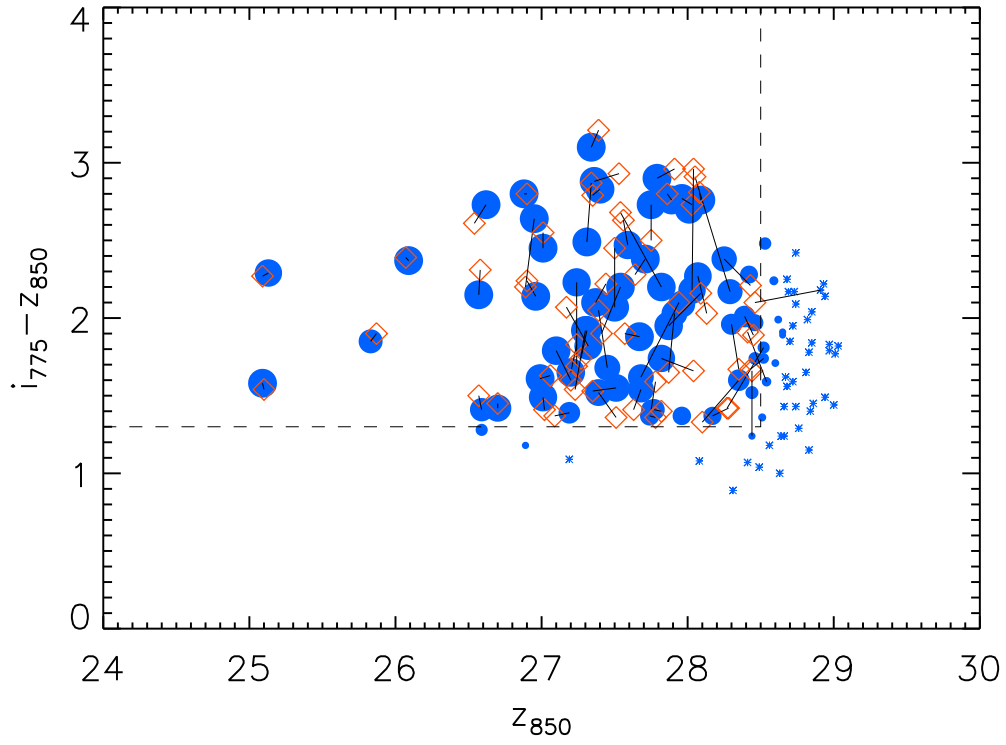


FIG. 3.— Color-magnitude diagram of the HUDF candidate pool. Candidates are indicated as filled circles whose radius is proportional to the f -factor, and asterisks are those objects with f -factor less than 0.2. The diamonds are i_{775} -dropouts selected in one realization for use in later ML process, and the line segments connect the cataloged and realized positions in the diagram.

TABLE 3
BINNED NUMBERS OF i_{775} -DROPOUTS IN
THE HUDF^a

$z_{850}^{(1)}$	$N_c^{(2)}$	$N_f^{(3)}$	$N_s^{(4)}$
24.75	0	0.00	0.01 ± 0.12
25.25	2	1.95	1.94 ± 0.25
25.75	1	0.83	0.84 ± 0.39
26.25	1	1.00	1.26 ± 0.50
26.75	8	8.42	8.11 ± 1.47
27.25	16	15.52	16.54 ± 1.98
27.75	21	19.22	18.07 ± 2.34
28.25	14	11.13	11.30 ± 2.19

^a for illustration only, not for later calculations.

(1) Central bin magnitude.

(2) Number of $i_{775} - z_{850} > 1.3$ i_{775} -dropouts from the catalog without corrections.

(3) Number of i_{775} -dropouts weighted with their f -factor.

(4) Number of i_{775} -dropouts in simulations considering f -factor.

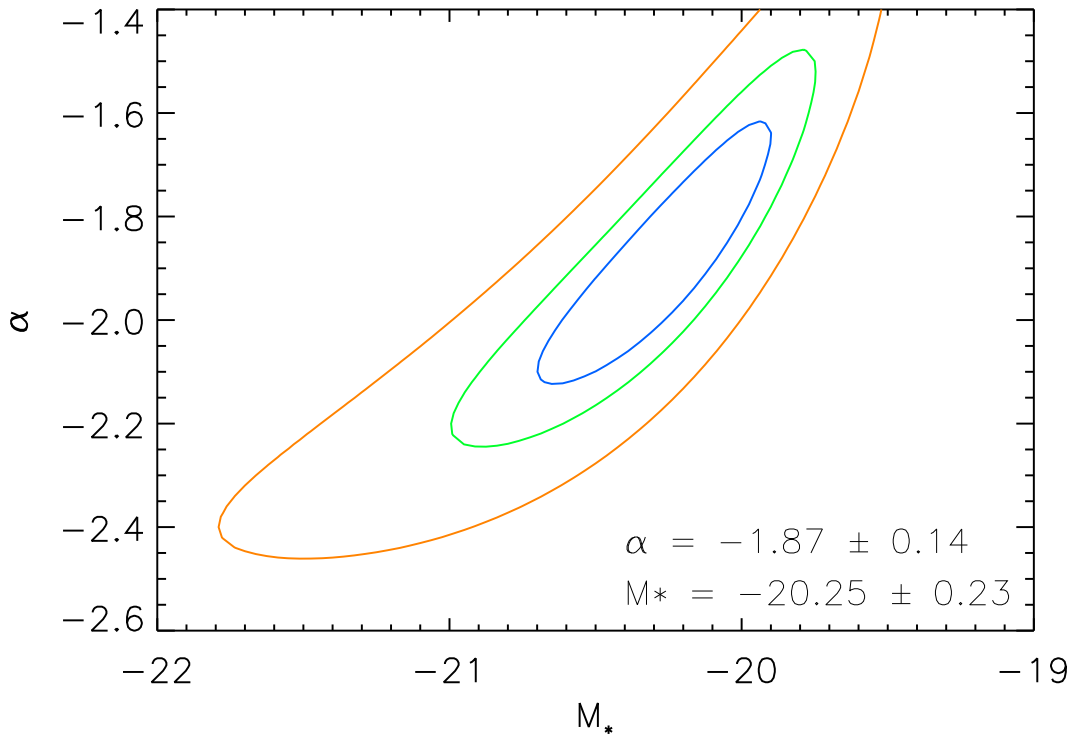


FIG. 4.— Likelihood contour for the best fit Schechter parameters of the $z \sim 6$ LF. The contours, inner to outer, stand for 1-parameter 1- σ , 2-parameter 1- σ , and 1-parameter 2- σ likelihood contours averaged over realizations for use in the ML process.

TABLE 4
STUDIES OF THE $z \sim 6$ LUMINOSITY FUNCTION

References	Fields ^a	N ^b	α	M_*
Bouwens et al. (2004)	UDF PFs (28.1)	30	-1.15	-20.26
Bunker et al. (2004)	HUDF (28.5)	54	≤ -1.60	-20.87
Dickinson et al. (2004)	GOODS (26.0)	5	-1.60 (fixed)	-19.87
Yan & Windhorst (2004)	HUDF (30.0)	108	(-1.90,-1.80) ^c	-21.03
Malhotra et al. (2005)	HUDF (27.5)	23 ^d	-1.80 (fixed)	-20.83
paper I	HUDF (29.0)	54	-1.60 (fixed)	-20.5
Bouwens et al. (2006)	HUDF (29.2) ... ^e	506	-1.73 ± 0.21	-20.25 ± 0.20
Bouwens et al. (2007)	HUDF (29.3) ... ^f	627	-1.74 ± 0.16	-20.24 ± 0.19
McLure et al. (2009)	UDS (26.0)	157 ^g	-1.71 ± 0.11	-20.04 ± 0.12
this work	HUDF (28.5) ... ^h	1164	-1.87 ± 0.14	-20.25 ± 0.23

^a The fields and z_{850} -band detection limit studied by the reference.

^b The number of candidates.

^c $-1.9 < \alpha < -1.8$.

^d all spectroscopically confirmed.

^e HUDF (29.2)+HUDF-Ps (28.5)+GOODS (27.5).

^f HUDF (29.3)+HUDF05 (28.9)+HUDF-Ps (28.6)+GOODS (27.6).

^g plus binned data points from Bouwens et al. (2007).

^h HUDF (28.5)+UDF05 (28.0)+GOODS (27.5)

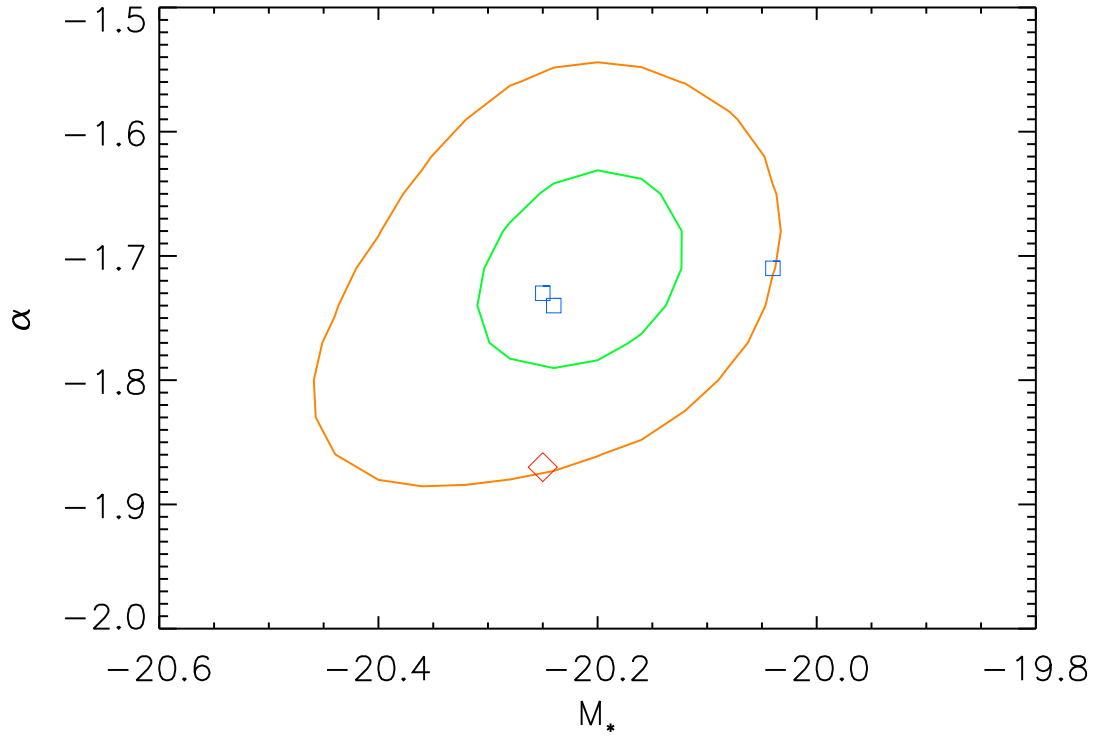


FIG. 5.— Most probable parameter space at $z \sim 6$ based on ten studies. The inner contour includes 68% probability and the outer 95%, assuming all the studies are independent and correct. Two nearby squares are from Bouwens et al. (2006, 2007), a third square is from McLure et al. (2009) who combine their data with Bouwens et al. (2007), and the diamond is from this work. As illustrated in Fig. 4, M_* and α are strongly correlated, so we do not plot their error bars, which can be found in Table 4.

TABLE 5
EVOLUTION OF THE LUMINOSITY DENSITY^a

	Reddy & Steidel (2009) ($z \sim 3$)	paper II ($z \sim 5$)	this work ($z \sim 6$)
M_*	-20.97 ± 0.14	-20.78 ± 0.21	-20.25 ± 0.23
α	-1.73 ± 0.13	-1.54 ± 0.10	-1.87 ± 0.14
ϕ_* ^b	1.71 ± 0.53	$0.9^{+0.3}_{-0.3}$	$1.77^{+0.62}_{-0.49}$
L_* ^c	$1.06^{+0.15}_{-0.13}$	$0.89^{+0.19}_{-0.16}$	$0.55^{+0.13}_{-0.11}$
LD0.3 ^d	$1.49^{+0.40}_{-0.33}$	$0.57^{+0.14}_{-0.12}$	$0.46^{+0.17}_{-0.13}$
LD0.2	$1.89^{+0.44}_{-0.38}$	$0.71^{+0.15}_{-0.14}$	$0.68^{+0.20}_{-0.16}$
LD0.04	$3.27^{+0.45}_{-0.38}$	$1.12^{+0.15}_{-0.14}$	$1.70^{+0.23}_{-0.21}$

^a See Fig. 7 for the graph.

^b in units of 10^{-3} Mpc^{-3} .

^c in units of $10^{29} \text{ erg s}^{-1} \text{ Hz}^{-1}$.

^d in units of $10^{26} \text{ erg s}^{-1} \text{ Hz}^{-1} \text{ Mpc}^{-3}$. LD0.3 means that the LD is integrated from $0.3L_*(z=3)/L_*(z)$.

TABLE 6
THE STEEPENING OF α BY THE FLUX
BOOSTING FOR $\sigma(m) \propto 10^{0.3(m-m_*)}$

	$\alpha = -1.5$	$\alpha = -1.7$	$\alpha = -1.9$
$S/N > 3$	0.14	0.18	0.26
$S/N > 5$	0.03	0.04	0.08
$S/N > 7$	0.01	0.02	0.03

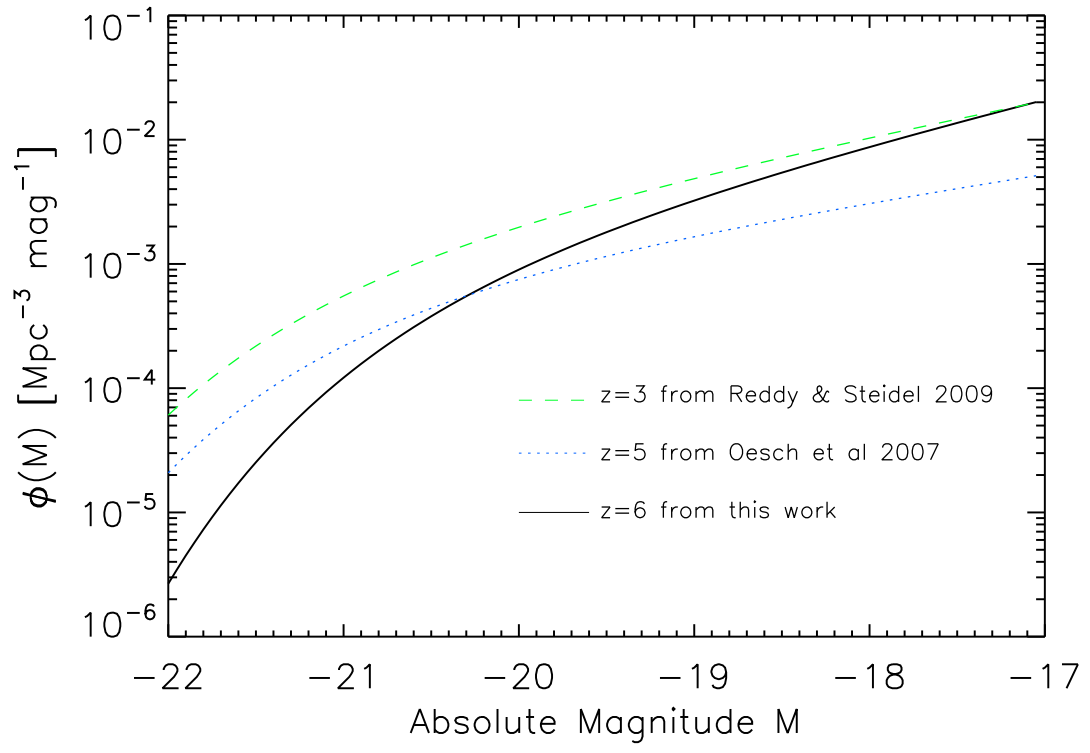


FIG. 6.— Luminosity function from $z \sim 3$ to $z \sim 6$.

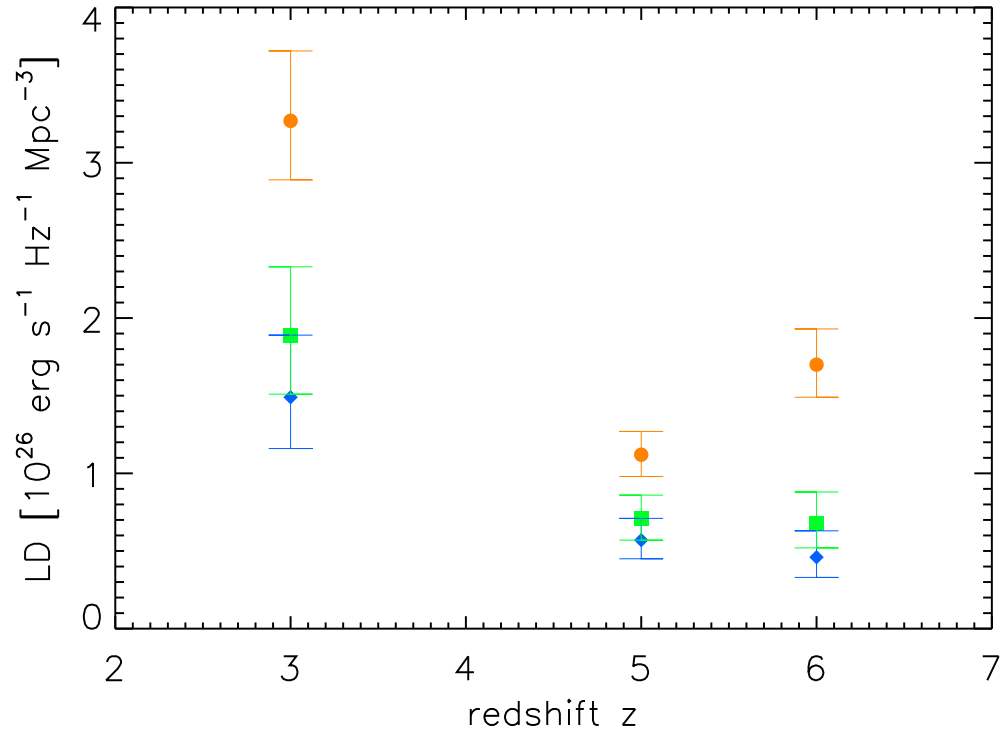


FIG. 7.— Luminosity density from $z \sim 3$ to $z \sim 6$ integrated to 0.3 (diamonds), 0.2 (squares), 0.04 (circles) of $L_*(z = 3)$. $z \sim 3$ data calculated from Reddy & Steidel (2009), $z \sim 5$ data calculated from paper II, and $z \sim 6$ data calculated from this work. See Table 5 for the numbers.